scientific reports

Check for updates

OPEN

Emerald eco-synthesis: harnessing oleander for green silver nanoparticle production and advancing photocatalytic MB degradation with TiO_2&CuO nanocomposite

Amira M. Shawky[1,4], Rania Elshypany[2,4], Heba M. El Sharkawy[2]✉, Mahmoud F. Mubarak[3] & Hanaa Selim[2]✉

The tertiary composite of TiO_2/CuO @ Ag (TCA) were synthesized by the solid state method using different ratios of TiO_2/CuO NCs and Ag NPs. The structural, morphological, and optical properties of nanocomposites were analyzed by scanning electron microscope, Transmission electron microscope, X-ray diffraction, Fourier transform infrared spectra, UV–Vis diffuse reflectance spectra (UV–Vis/DRS) and photoluminescence spectrophotometry. The results showed enhanced activity of TCA hybrid nano crystals in oxidizing MB in water under visible light irradiation compared to pure TiO_2. The photocatalytic performance TCA samples increased with suitable Ag content. The results show that the photo degradation efficiency of the TiO_2 compound improved from 13 to 85% in the presence of TiO_2–CuO and to 98.87% in the presence of Ag containing TiO_2–CuO, which is 7.6 times higher than that of TiO_2. Optical characterization results show enhanced nanocomposite absorption in the visible region with long lifetimes between e/h+ at optimal TiO_2–CuO/Ag (TCA_2) ratio. Reusable experiments indicated that the prepared TCA NC photo catalysts were stable during MB photo degradation and had practical applications for environmental remediation.

Currently, the issue of energy crisis and environmental pollution is a topical and global issue, and solving these problems by different methods has been of particular interest[1,2]. The carcinogenic organic dyes are commonly used in the manufacture of various products as plastics, paper, textiles and paints. The wastewater discharged by these industries has serious impacts on the environment and on the health of humans and other organisms[3]. Most of these dyes are of synthetic origin and often include aromatic rings in their molecular structure, which are inert and cannot be degraded when released in wastewater without proper treatment[4,5]. Therefore, from the point of view of protecting human health and environmental resources, it is very urgent to remove such dyes from contaminated water[6]. Methylene blue (MB), the most commonly used basic dye, is thought to have a variety of uses in the printing and dyeing industry[7]. For this reason, several strategies have been described to remove MB from aqueous solutions, such as photocatalytic, biological and other conventional methods[8–10]. Among the methods utilised, photocatalysis is one that removes pollutants in an attractive and efficient approach[11,12]. One of the most promising methods to clean the environment is the photocatalytic removal of pollutants utilizing high performance semiconductor catalysts[13]. One of the most promising methods to clean the environment is the photocatalytic removal of pollutants via utilizing high performance semiconductor catalyst such as Titanium dioxide (TiO_2)[14]. However, the applicability of TiO_2 has been constrained due to poor photocatalytic activity in the visible area caused by the broad band gap (3.2 eV)[15]. In order to solve this issue and enhance the

[1]Sanitary and Environmental Institute (SEI), Housing and Building National Research Center (HBRC), Giza 1770, Egypt. [2]Department of Analysis and Evaluation, Egyptian Petroleum Research Institute, Nasr City, Cairo 11727, Egypt. [3]Department of Petroleum Application, Core Lab Analysis Center, Egyptian Petroleum Research Institute, P.B. 11727, Nasr City, Cairo, Egypt. [4]These authors contributed equally: Amira M. Shawky and Rania Elshypany. ✉email: h_magdy54@yahoo.com; dr.hanaa_epri@hotmail.com

photocatalytic activity of TiO_2, multiple approaches have been attempted, such as doping[16], surface modification[17] or a combination of semiconductor oxides[18]. Considering such modifications, visible light can be used to create electron-holes and extend their separation time, enhancing the photocatalytic activity[19]. Copper oxide (CuO) nanoparticles, are among the metal oxides, which have a band gap energy of 2.1 eV[18], have drawn a lot of attention because of their low cost, nontoxicity, good optical and catalytic capabilities, and superior activity in the visible spectrum[20,21]. In order to degrade Rhodamine B by UV–visible light, Ravishankar et al. used CuO/TiO_2 nanocomposite as a photocatalyst. Under ideal circumstances, 98% of Rhodamine B dye was degraded in the presence of this nanocomposite. Bathla and colleagues reported the use of CuO/TiO_2 nanocomposite to remove methyl orange dye when exposed to sunlight. They degraded that after 8 h of exposure to sunlight[22]. Bae et al. investigated the photocatalytic activity of hollow CuO/TiO_2 nanospheres for the degradation of methylene blue. According to their findings, the photocatalytic performance of the nanospheres enhanced when exposed to visible light, and 90% of the methylene blue was destroyed[23]. Silver nanoparticles (SNP) have drawn a lot of interest because of their superior catalytic abilities during the dye oxidation process. SNP synthesis is often accomplished using a variety of physicochemical techniques. The majority of these methods have been demonstrated to be effective for the creation of SNP. However, they come with built-in drawbacks such the need for expensive chemicals, corrosive nature, and potential dangers to the environment. Utilizing an environmentally friendly strategy that involves organic SNP synthesis using plant-based extracts may be the solution to these negative consequences[24,25]. Numerous physical and chemical processes result in the production of nanoparticles that are hazardous or harmful for the environment. The biological approach and green chemistry are two common safer methods used by researchers to create nanomaterials[26]. Because it is so simple to manipulate, the green chemistry method has been widely used for the quick synthesis of AgNPs[27]. Researchers are adopting environmentally friendly processes to synthesise a variety of metallic nanoparticles since there is an increasing need for environmentally friendly nanoparticles. However, plant extract has been employed as a reducing agent to create nanoparticles that may be useful for the time being[26]. This study focusing on the effectiveness of prepared a novel silver nanoparticles by green chemistry from *Nerium oleander* as photocatalyst and enhanced its activity with nanocomposite TiO_2@ CuO for MB photo-degradation in water by visible light irradiation.

Experimental

Materials

The chemicals used in this work are: Titanium (IV) isopropoxide (TIPO) [$Ti(OCH(CH_3)_2)_4$], copper nitrate tri hydrate $Cu(No_3)_2$ $3H_2O$ and silver nitrate $AgNO_3$ are supplied by Sigma-Aldrich companies. Sodium hydroxide (NaOH) of purity (99%), Ethanol, methylene blue dye were purchased from Merck KGaA (Darmstadt, Germany) and Nerium oleander leaves. All solutions were made with fresh deionized water. All chemicals used in this work were of analytical grade and were used without further purification. The Study complies with local and national regulations and guidelines.

Nanoparticles synthesis

Synthesis of TiO_2 nanoparticles (T)

TiO_2 NPs were prepared using a sol–gel method[5]. In a typical synthesis, an appropriate amount of Ti-isopropoxide precursor was mixed with deionized water and dissolved in 87.5 mL of ethanol, stirred at room temperature for 4 h, washed several times with deionized water, and dried at 90 °C. Finally, the obtained powder was calcined in air in a muffle furnace at 500 °C for 1 h to extract TiO_2 NPs.

Synthesis of CuO nanoparticles (C)

CuO nanoparticles were prepared by a precipitation method[28]. A solution of $Cu(No_3)_2$ $0.3H_2O$ (0.1 M) was dissolved in 100 mL of distilled water with continuous stirring. Add 0.1 M NaOH to the above solution until the pH reaches7. The color of the solution immediately changed from light blue to black and a large amount of black precipitate was formed. The precipitate was centrifuged and washed 3–4 times with deionized water. The resulting precipitate was air dried for 24 h. This CuO powder was used to characterize the material.

Synthesis of TiO_2&CuO nancomposite (TC)

A TiO_2/CuO nanocomposite (TC) was synthesized by a solid-state method[29]. TiO_2/CuO composites were prepared using different weight ratios of T:C (0.1:0.08, 0.1:0.1, and 0.1:0.12 wt%) labeled as TC_1, TC_2, and TC_3, then milled together, sonicated in a prope sonicator for 15 min. It was washed for several minutes, and then calcinated at 400 °C for 4 h.

Preparation of Ag NPs by green synthesis

Preparation of $AgNO_3$ solution. 0.5 g of $AgNO_3$ was dissolved in distilled water (50 mL), then the solution was stirred at 60–70 °C for 15 min. until it is homogeneous. The solution is stored in a dark container to avoid oxidation.

Preparation Nerium oleander leaves extract. The oleander leaves were washed with water several times, sterilized with 50% ethanol to remove foreign substances such as dust, washed with distilled water several times, and cut into 25 cm pieces. An equal amount of gram pieces of oleander leaves was mixed with 100 ml of distilled water and boiled in a sterile flask at 80–90 °C for 5–10 min. until the water turned green color. The solution was filtered and stored in a refrigerator at 3 °C[30].

Synthesis of silver nanoparticles (A). For the synthesis of AgNPs, a certain amount of oleander extract (1 mL) was dropped into a suitable amount of $AgNO_3$, and the aqueous solution was heated at 80 °C for 15 min. The resulting solution was pale yellow, indicating the formation of AgNPs.Hence; nerium oleander leaves extract was used as a bio-functional reducing material for the green synthesis of silver nanoparticles (Ag NPs)[31].

Synthesis of TiO_2&CuO @ Ag nancomposite (TCA)
A TiO_2/CuO/Ag nanocomposite (TCA) was synthesized by a solid-state method. The optimal ratio of TC composite and Ag was established by using different weight ratios of TC:A (0.1:0.03, 0.1:0.05, and 0.1:0.06 wt%) are mentioned as TCA_1, TCA_2, and TCA_3, and then milled together, sonicated for 15 min. Washed several times by distilled water and ethanol, and calcined at 400 °C for 4 h.

Experimental techniques

The morphology of the prepared materials was examined with a scanning electron microscope (SEM) (JEOL) and a JEOL transmission electron microscope (TEM) associated with selected area electron diffraction (SAED). The phases of the prepared samples were examined by his X-ray diffraction (XRD) using a diffractometer (Panalytical XPERT PRO MPD). CuKα radiation (λ = 1.5418 Å) was used at 40 kV and 40 mA. Functional groups were identified in the wavenumber range 400–4000 cm^{-1} using a Fourier transform infrared (FT-IR) spectrometer model Spectrum One (Perkin Elmer, USA). Light reflectance was recorded using a UV–Vis spectrometer (Perkin Elmer Lambda 1050). Photoluminescence spectra were recorded on a Cary Eclipse fluorescence spectrophotometer.

Photocatalytic activity study

The photocatalytic decomposition activity was examined using a photoreactor equipped with a 400 W halogen lamp as light source. The distance between the halogen lamp and the dye solution is 10 cm. Then, 0.025 g of photocatalyst was added to 30 ml of 20 ppm MB dye solution, and the solution was stirred in the dark for 30 min to reach adsorption–desorption equilibrium. Photolysis was started in 120 min and 5 ml of suspension was obtained in 30 min. The obtained suspension was analyzed by UV–Vis spectrophotometer at the MB solution's maximum absorption wavelength of 664 nm[32].

Results and discussion

The SEM images of the most efficient photocatalyst of (0.05%) TiO_2/CuO@Ag nanocomposite (TCA_2), TC_1 and pure TiO_2, CuO nanoparticles are shown in Fig. 1. The SEM image of pure anatase TiO_2 grains has rounded shape and form sponge-like aggregates as presented in Fig. 1a, and the global and uniform particles indicated in images of CuO and TC_1 are coherent together as shown in Fig. 1b,c. There was also a higher tendency of agglomerations. In Fig. 1d indicates the SEM graph of net composite TiO_2/CuO@ Ag, hence; the composite of TiO_2 with CuO

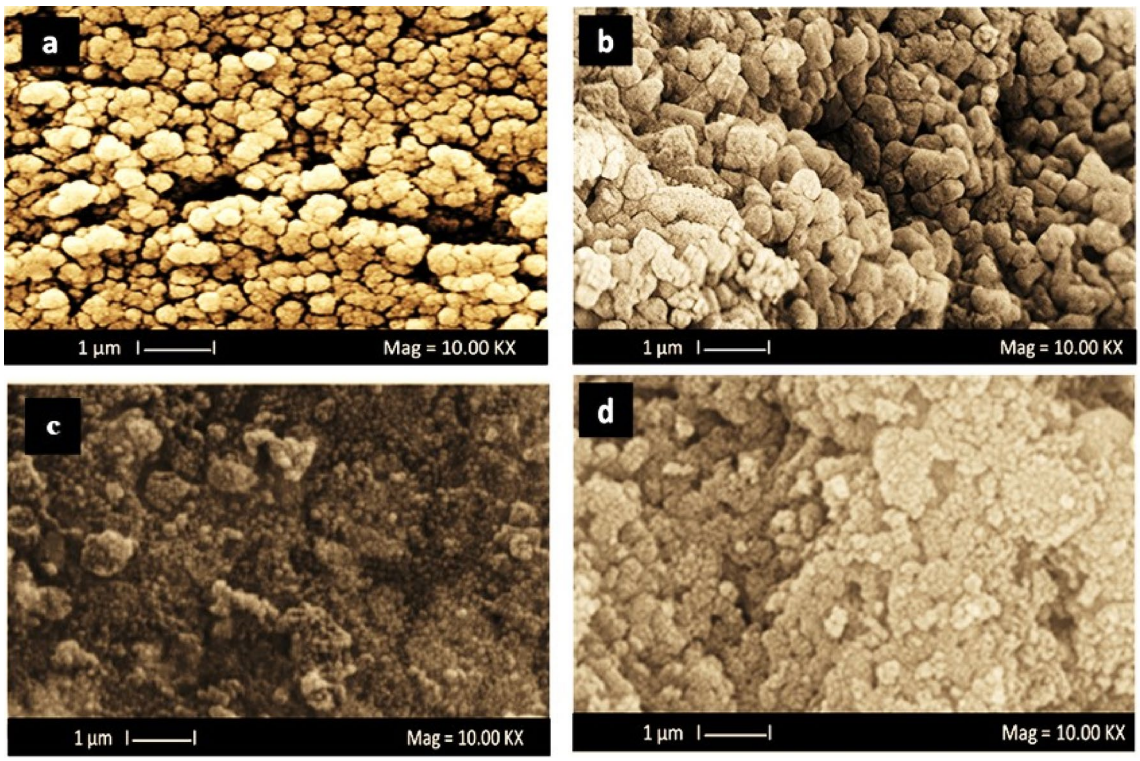

Figure 1. SEM images of the pure TiO_2 (**a**), CuO (b), TC_1 (**c**); and TCA_2 (**d**) nanocomposites.

appears also spherical shapes and Ag nanoparticles with even shape and spherical nature, which aggregated on the surface of the composite. This evident the composite is successfully prepared.

The TEM micrographs of the pure and composite samples are represented in Fig. 2. The figure shows that nanoparticles have almost spherical shape corroborating the images of the SEM. Other essential results can be gotten from Fig. 2 is that the particle sizes of the TC are more aggregated than that found for pure one. While the TCA composite the sliver was appeared as Irregular sphere. Moreover, a series of bright diffraction rings were observed through the corresponding ring pattern of the selected-area electron diffraction (SAED), suggesting the polycrystalline nature of the prepared material, Fig. 2e–h.

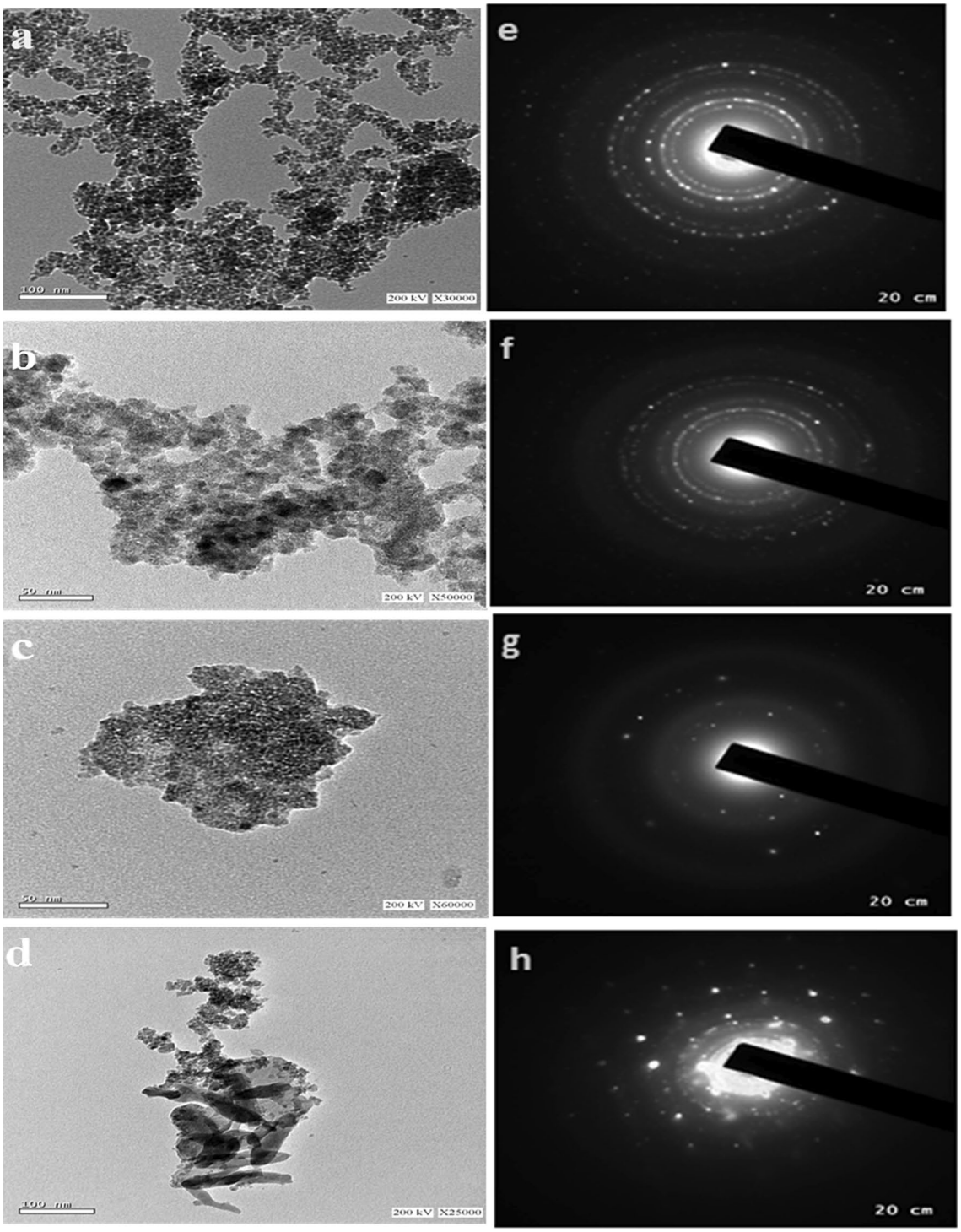

Figure 2. TEM images of the pure TiO_2 (**a**), CuO (**b**) TC_1 (**c**); and TCA_2 (**d**) nanocomposites; and their SAED patterns (**e**–**h**), respectively.

The X-ray diffraction spectra was used to illustrate the purity, crystal structure and the phase formed for the as prepared nanocomposites. Figure 3 was displayed the X-ray diffraction spectra of bare samples of TiO_2, CuO, and Ag along with nanocomposites of TiO_2/CuO and TiO_2/CuO@Ag with different weight percentages of CuO and Ag, respectively. The diffraction peaks at 2θ of 26.69°, 36.13°, 50.05° and 54.40° corresponding to lattice planes (101), (004), (200) and (105), respectively for TiO_2 anatase structure. Additionally, diffraction peaks characteristic to monoclinic CuO were noticed at 2θ of 35.44°, 38.81° and 48.70° representing to planes (110), (111) and (202), respectively. Upon adding CuO with various ratios of TiO_2 the resultant nanocomposits (TC) contain mixed diffraction peaks of both CuO, TiO_2 and the intensity of peaks of TiO_2 was slightly decreased without the observation of any foreign peaks, conforming the successful formation of TC composites with high purity as shown in Fig. 3a. Furthermore, the main peaks of nano silver appeared at 2θ values of 38.02°, 44.37°, 64.32°, and 77.22° corresponding to planes of (111), (200), (220) and (311), respectively. Figure 3b revealed the Bragg reflections of silver after addition of Ag to TC composites with different ratios, new main peaks were detected approximately at 2θ of 43.58°, and 64.32°, and 77.22° which indexed well with the XRD patterns of Ag nanoparticles. It is noted that the diffraction peaks have some sharpness, demonstrating the great crystallinity of the prepared photocatalysts.

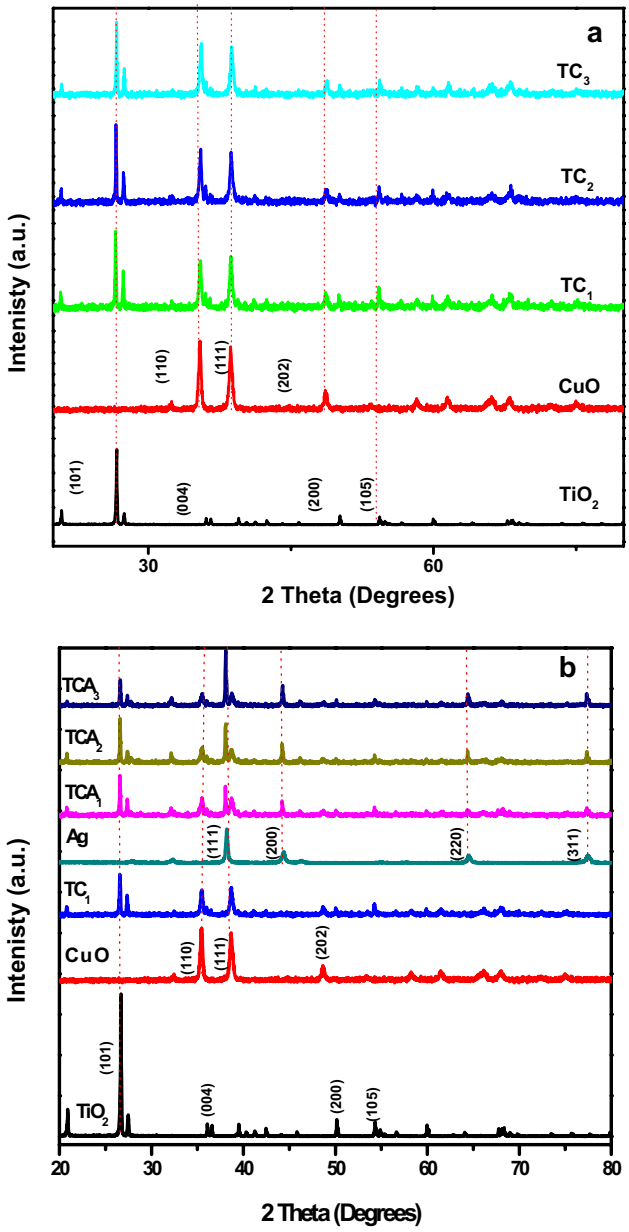

Figure 3. XRD pattern of TiO_2 and CuO with (**a**) TC_1, TC_2 and TC_3; and (**b**) TCA_1, TCA_2 and TCA_3 nanocomposites.

Figure 4 shows the FT-IR spectra of TiO_2, CuO and TiO_2/CuO @ Ag composite photocatalysts with mole ratios of Ag of 0%, 0.03%, 0.05%, and 0.06% for TC_1, TCA_1, TCA_2 and TCA_3 nanocomposites, respectively. The FT-IR spectrum of TiO_2 shows strong absorption bands in the range of 400–700 cm^{-1}. This band is assigned to the stretching vibration of the Ti–O–Ti bond and indicates the formation of TiO_2 at 646 cm^{-1}[33]. In Fig. 4a, the FT-IR spectrum of CuO shows peaks at 718.49, 848.53 and 960.67 cm^{-1} revealed the formation of CuO. A broad peak noticed at 3371.57 cm^{-1} attributed to O–H stretching of the moisture content[34]. For TC spectrum shows the presence of CuO oxide will give two characteristic low-intensity peaks of CuO vibrations in the 400–800 cm^{-1} region[35]. However, the spectrum of TiO_2 will appear in the same region 400–800 cm^{-1}, two high intensity peaks appeared for Ti–O vibrations[36]. It is easy to predict that the high-intensity characteristic peaks of TiO_2 will overlap the low-intensity characteristic peaks of CuO in this wavenumber region. That is why there is no difference in characteristic peaks in the presence or absence of CuO oxide in the photocatalysts. Figure 4b revealed the FT-IR spectra of TiO_2–CuO/Ag nanocomposites, which show all the characteristic vibrations of TiO_2, CuO and silver, characteristic absorption peak at 1090.72,801.81, 690.40,504.43and 476.31 cm^{-1}, hence; the peaks observed at 1090.72, and 960.67 cm^{-1} indicate the presence of silver nanoparticles[37]. Based on these results, a photocatalyst was prepared that did not contain any unnecessary foreign substances.

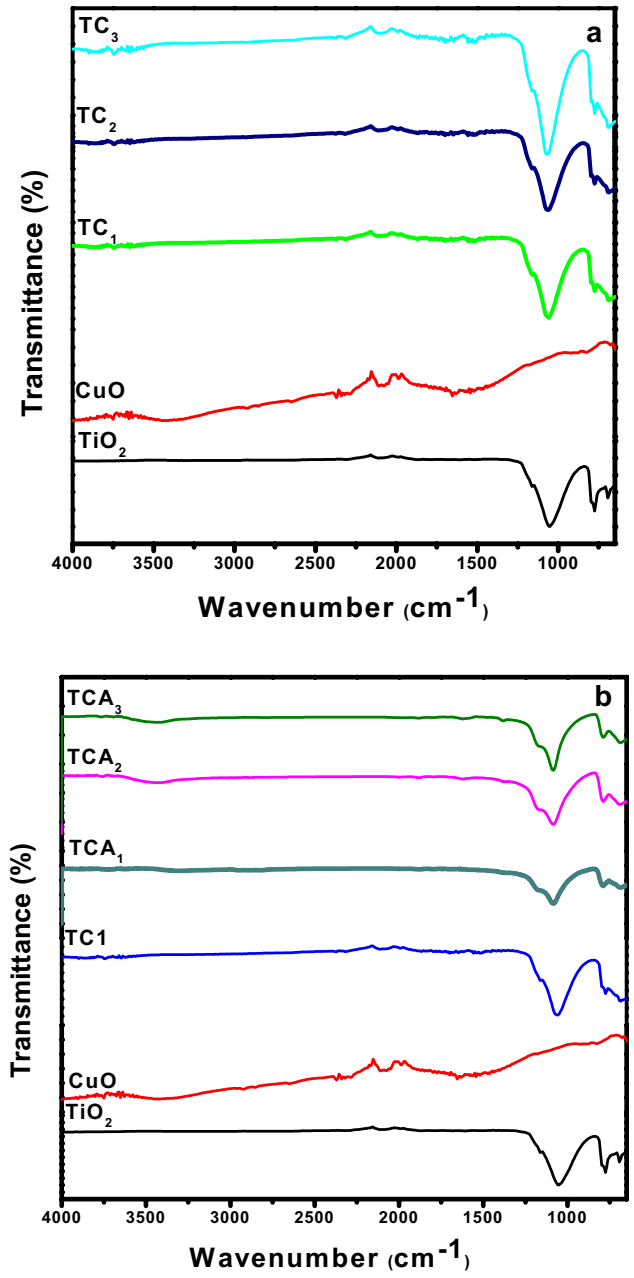

Figure 4. FT-IR Spectra of TiO_2 and CuO with (**a**) TC_1, TC_2, and TC_3; and (**b**) TCA_1, TCA_2 and TCA_3 nanocomposites.

The photocatalytic performance of a semiconductor significantly depends on its optical property, and thus, it is one of the important factors which should be studied. Figure 5a shows typical diffuse reflectance spectroscopy (DRS) curves for optical absorption behavior of pristine TiO_2 and CuO and their composites TC_1, TC_2, and TC_3 in the range of 200–800 nm. It was observed that the Pure TiO_2 photocatalyst displayed almost the strongest absorption intensity at 422 nm compared with its counter parts. Furthermore, the pristine CuO nanocomposite showed relatively small absorption band edge around 270 nm that is compatible with the small band gap of CuO 1.3 eV. As for TC_1, TC_2 and TC_3 NCs, It can be seen the low intensity of reflectance, indicating the highly absorbance of light in visible range based on the reduction of the band gap energy. It is proposed that the combination of n-type and p-type semiconductors produces an internal electric field, resulting in the production of a p-n hetero junction. The creation of this p-n hetero junction, as well as the band alignment between CuO and TiO_2, considerably facilitates electron–hole separation and increases catalytic activity[38–40]. Next, the best performing photocatalyst, TC_1 was modified with Ag nanoparticles as shown in Fig. 5b. Hence; Ag NPs modification of photocatalysts TCA_1, TCA_2 and TCA_3 endowed the TiO_2/CuO @ Ag ternary composites the lowest reflectance, the optimum composite TCA_2, as a result of the synergetic effect among components[41,42]. It has been demonstrated that lowering the composite's band gap energy improves the photocatalytic reaction by allowing the produced photocatalyst to absorb more photons and become more sensitive to visible light. The conjugation of two bands gap increased the stability between the e^-/h^+ pairs.

The PL spectra demonstrate the behavior of photo generated charge carriers (e^-, h^+),where a low recombination rate of photogenerated electrons and holes means a good separation between (e^-, h^+), a low fluorescence intensity in PL spectra and consequently excellent photo degradation performance. Figure 6a,b displays the PL measurements of TiO_2, CuO, TC, and TCA nanocomposites[43]. The bare photocatalys, CuO, TiO_2, and their

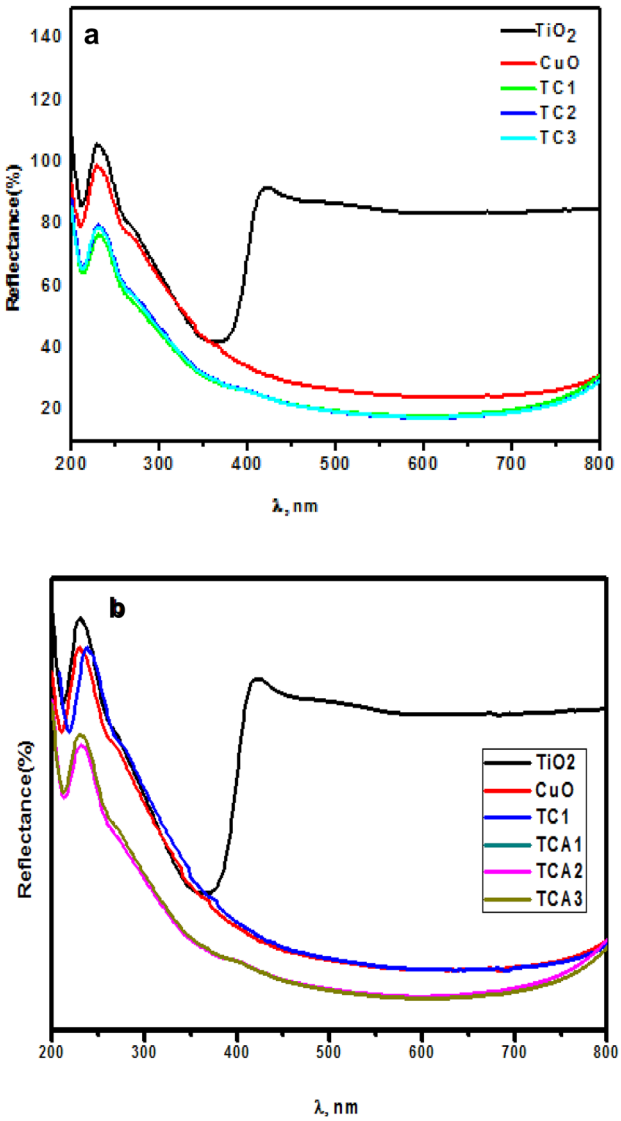

Figure 5. UV–Vis diffuse réflectance spectra of TiO_2 and CuO with (**a**) TC_1, TC_2 and TC_3; and (**b**) TCA_1, TCA_2 and TCA_3 NCs.

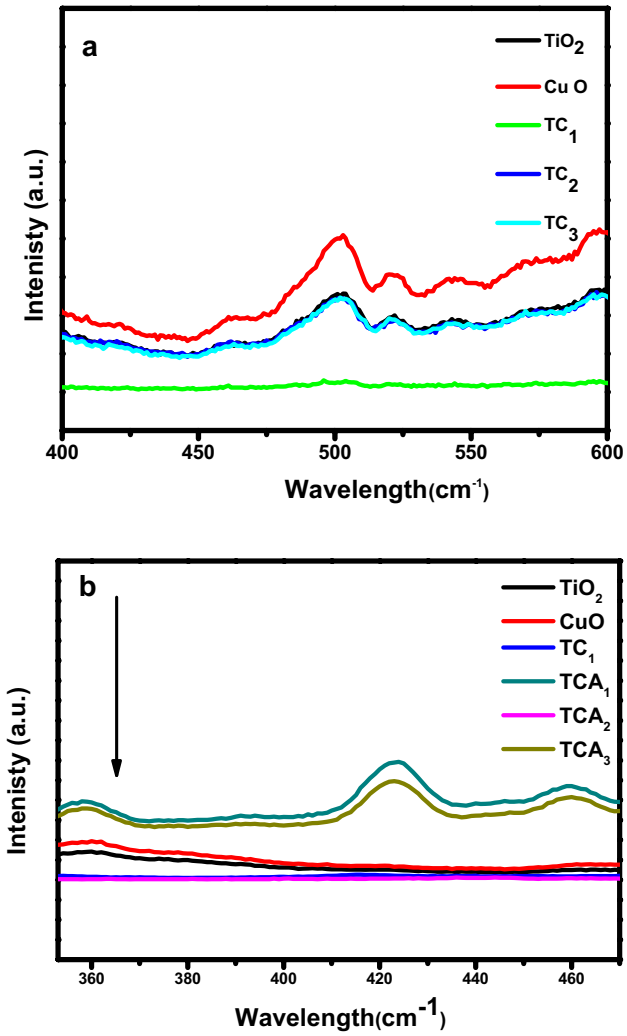

Figure 6. (**a**) Photoluminescence spectra of TiO_2 and CuO with TC_1, TC_2, TC_3; and (**b**) TCA_1, TCA_2 and TCA_3 NCs.

nanocomposites (TC_1, TC_2, TC_3) exhibte emission peaks around wavelength range of 470 to 550 cm^{-1}, referring the recombination of photogenerated charge carriers in visible light region as shown in Fig. 6a. Moreover, a strong PL quenching is observed for TC_1, TC_2, and TC_3 nanocomposites. TC_1 photocatalyst displays the smallest PL intensity, indicating that the recombination between photo-electrons generated and holes is reduced[44]. Remarkably, Fig. 6b reveals the PL emission of TCA ternary composite, TiO_2/CuO @ Ag NCs was further quenched after the addition of Ag nanoparticles to extremely low intensity, indicating improved carriers life time and effective electron hole separation. The p-n heterojunction of CuO/TiO_2 align with the Schottky junction created with metallic Ag are responsible for facilitating charge separation and transfer through the interfaces[45]. Hence, TCA_2 nonocomposite represents a lower recombination rate provides greater dye degradation efficiency for the photocatalyst, consistent with the photocatalytic results.

Using MB dye as a model pollutant, the photocatalytic activity of the produced TiO_2, TC and TCA nanocomposites was examined as demonstrated in Fig. 7a,b. The photocatalytic efficiency of MB decomposition was calculated from the Eq. (1):

$$D\ \% = (C_0 - C/C_0) * 100 \quad (1)$$

where C_0 is the initial concentration and C is the remaining concentration of MB after the reaction. Initially, to reach adsorption/desorption equilibrium, the solution was held in the dark for 30 min prior to light irradiation. On the other hand, it is obvious that the photocatalytic performance of pure TiO_2 was lower than that for their composites (TC) during the irradiation times of 0, 30, 60, 90, 120 and 150 min. This attributed to the large band gap of TiO_2, it suffer from high rate recombination between the photo induced charge carriers (e^-, h^+)[46]. Form Fig. 7a revealed the combination of TiO_2 and CuO the photocatalytic activity increases to reach (85%) for TC_1 photocatalyst compared to pure TiO_2 (13%), TC_2 (79%) and TC_3 (78%). Furthermore, maximum degradation efficiency was obtained by inclusion of a suitable portion of Ag nanoparticles to TC_1 in the composite TiO_2/

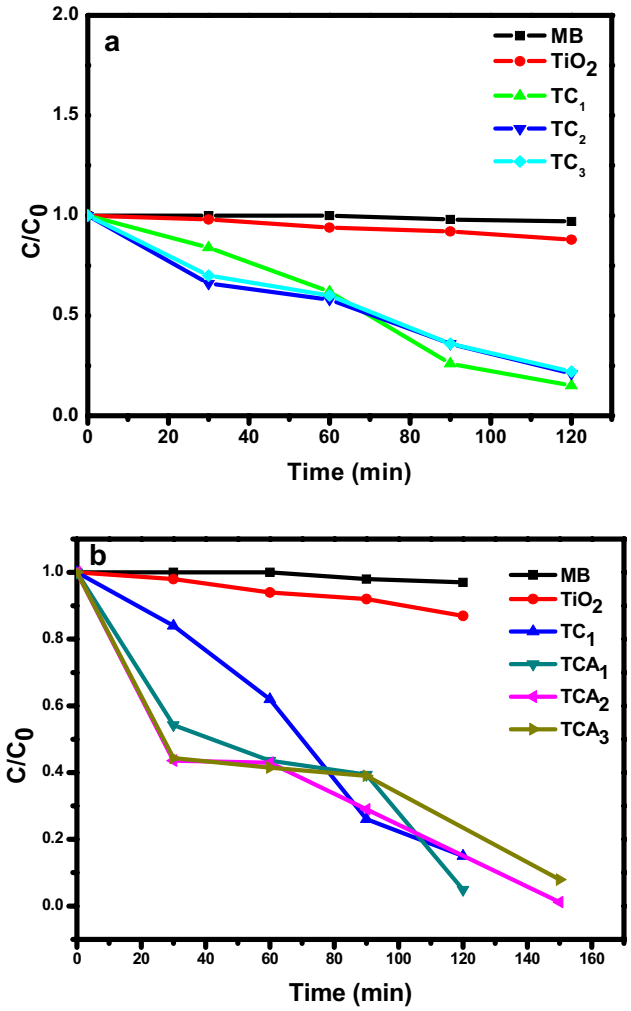

Figure 7. Photocatalytic degradation of MB by TiO_2 (**a**) TC_1, TC_2, TC_3; and (**b**) TC_1, TCA_1, TCA_2 and TCA_3 NCs.

CuO @ Ag NCs with a degradation efficiency reach to (98.87%) for TCA_2 as shown in Fig. 7b. The higher photo catalytic degradation efficiency of TCA_2 to MB dye may be related to a suitable amount of Ag nanoparticles in the composite resulting in a lower band gap energy and sufficient PL characteristic. Additionally, the lower and higher amount of Ag nanoparticles in the ternary composite, TCA, was exhibited a negative effect on photo-degradation performance as for TCA_1 and TCA_3 with photo degradation activity of (95.06%) and (92.07%), respectively. Where the lower Ag loading may be delay the transfer of photo generated carriers while the higher Ag loading may be hinder the light absorption.

The pseudo-first-order kinetic reaction of MB dye photodecomposition under visible light irradiation was explored in Fig. 8 and Table 1. The degradation kinetics of MB by the synthesized photo catalysts was calculated according to Eq. (2):

$$\ln(C_0/C) = k_a * t \quad (2)$$

where C_0 is the initial concentration (mg L^{-1}), C is the reaction concentration of the MB solution at time (t), and k_a is the rate constant (min^{-1}).

The linear relationship between the photodegradation time and dye concentration in the ln C_0/Ct versus t time (t) plot implies that the degradation process was pseudo-first-order and, photocatalytic rate constant can obtained from it as shown in Fig. 8a. Further, the super photocatalytic performance of TCA_2 is proofed from the photocatalytic rate constant value. It could be realized from Fig. 8b and Table 1 that the photocatalytic rate constant of nano composites (TC_1, TCA_1, TCA_2 and TCA_3) was more than that of pristine bare TiO_2 taking the order of TCA_2 (0.0315 min^{-1}) > TCA_1(0.02137 min^{-1}) > TCA_3 (0.01741 min^{-1}) > TC_1 (0.01655 min^{-1}) > T (0.00112 min^{-1}) > MB (0.0001min^{-1}). Additionally, adding Ag nanoparticles to TC1 photocatalyst was resulted in increased k_a value. The greatest rate constant (0.0315 min^{-1}) belongs to the TCA_2 photo catalyst. Which is consistent with the results of photocatalytic degradation, signifying that the catalyst has good features toward MB degrading activity under visible light.

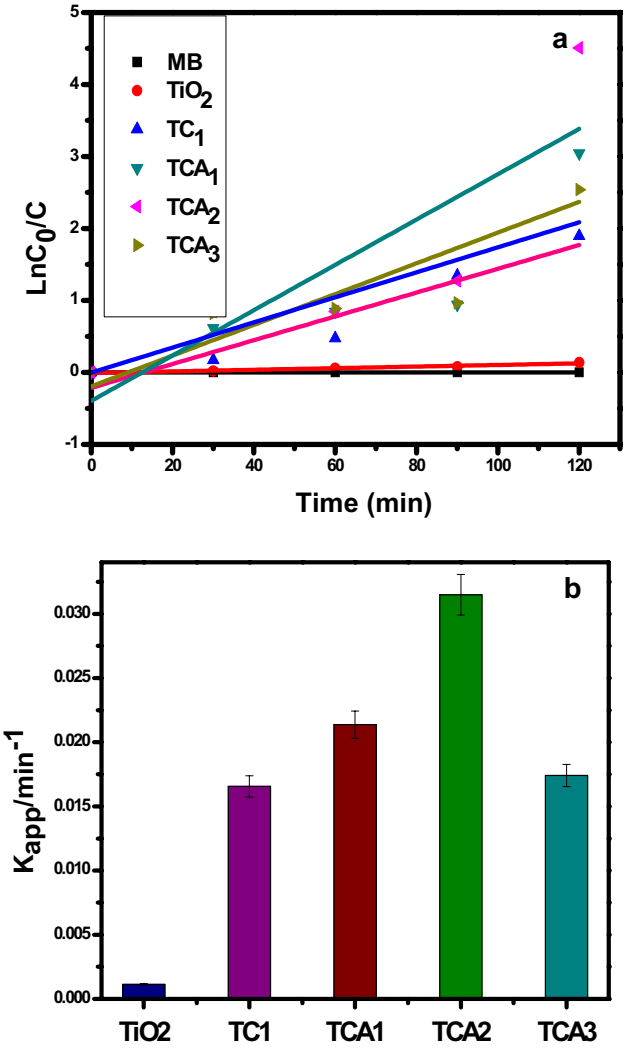

Figure 8. (**a**) Kinetics and; (**b**) apparent rate constants of MB degradation of by TiO_2 with TC_1, TCA_1, TCA_2 and TCA_3 NCs.

Sample	K_a
MB	**0.0001**
TiO_2	**0.00112**
TC_1	**0.01655**
TCA_1	**0.02137**
TCA_2	**0.0315**
TCA_3	**0.01741**

Table 1. The rate constant of nanocomposites (TiO_2, TC_1, TCA_1, TCA_2 and TCA_3). Significant values are in bold.

Table 2 provides a comparison of the photocatalytic efficiency of various catalysts in the degradation of a dye called Methylene Blue (MB) with respect to a synthesized nano-composite called TiO_2/CuO @ Ag. The table provides information on the photocatalyst, dye concentration, catalyst dose, preparation method, degradation percentage, and the corresponding reference for each entry.

The Ag@Cu_2O–CuO/TiO_2 catalyst was prepared using the sol–gel technique. It was tested against MB dye at a concentration of 20 ppm, with a catalyst dose of 0.5 g/L. The degradation percentage achieved was 83.00%[42]. Additionally, CuO-TiO_2 catalyst was synthesized using a green synthesis method involving *C. benghalensis* plant extracts. The MB dye concentration used was 20 ppm, and the catalyst dose was 1 g/L. The degradation achieved was 33.00%[47]. Also, the catalyst of Ag@CuO that prepared using an apolyol-mediated refluxing method, was

Photocatalyst	Dye type	Dye concentration (ppm)	Catalyst dose (g/L)	Preparation methode	Degradation (%)	Ref.
Ag@Cu_2O CuO/TiO_2	MB	20	0.5	Sol–gel technique	83.00	[42]
CuO-TiO_2	MB	20	1	Green synthesis usingC.benghalensis plant extracts	33.00	[47]
Ag@CuO	MB	20	2	Apolyol-mediated refluxing method	94.43	[42]
Ag/TiO_2/$CuFe_2O_4$	MB	5	1	Hydrothermal method	85,00	[48]
TiO_2@$CoFe_3O_4$	MB	100	1.0	Co-preciptation method	91,00	[5]
Pt/ZnO-MWCNT	MB	100	0.4	sol–gel method	74,00	[47]
Ag@CuO/TiO_2	MB	20	0.5	Green synthesis using nerium oleander leaves extract	98.87	This work

Table 2. Comparison of photocatalytic efficiency of relevant catalysis with respect to our synthesized TiO_2/CuO @ Ag nano-composite.

tested against MB dye at a concentration of 20 ppm with a catalyst dose of 2 g/L. It achieved a degradation percentage of 94.43%[42]. Furthermore, the hydrothermal method was used to synthesize of Ag/TiO_2/$CuFe_2O_4$ photocatalyst and then tested against MB dye at a concentration of 5 ppm, with a catalyst dose of 1 g/L. The catalyst exhibited degradation efficiency of 85.00%[48]. The degradation efficiency of 91% was achieved via TiO_2@$CoFe_3O_4$ nanocomposite against MB dye at a concentration of 100 ppm, with a catalyst dose of 1.0 g/L. TiO_2@$CoFe_3O_4$ catalyst was synthesized using the co-precipitation method[5]. The sol–gel method was further used to prepare Pt/ZnO-MWCNT catalyst and tested against MB dye at a concentration of 100 ppm, with a catalyst dose of 0.4 g/L, achieving 74%[47]. Finally, Ag@CuO/TiO_2 nano-composite that synthesized for the current work. The MB dye concentration used was 20 ppm, and the catalyst dose was 0.83 g/L. It was prepared using a green synthesis method involving nerium oleander leaves extract. The degradation achieved by this composite was 98.87%. In summary, the table compares the photocatalytic efficiency of relevant catalysts, including the TiO_2/CuO @ Ag nano-composite synthesized in the current work. It demonstrates that the TiO_2/CuO @ Ag composite showed the highest degradation percentage (98.87%) among all the tested catalysts for the degradation of MB dye at a concentration of 20 ppm and a catalyst dose of 0.5 g/L.

Reusability experiments were conducted using FT-IR after 120 min of photocatalysis, as can be seen in Fig. 9a. There was no change in the peak position, and the peaks exactly matched those of the FT-IR catalysis from before the photocatalytic degradation reaction. These findings explain how the produced catalyst can keep its stability and catalytic effectiveness even after numerous repeat usage. As demonstrated in Fig. 9b, the optimized photocatalyst TCA_2 for MB degrades at a rate that can be recycled, and after six cycles of usage, its photo degradation activity was found to slightly decline, showing strong stability. The interaction of TiO_2@CuO and Ag, which can immobilize silver nanoparticle active sites in photocatalysis, is responsible for stability feature of TCA NCs.

The photocatalytic dye degradation process includes light absorption, generation of electron–hole pairs, and redox reactions with the dye adsorbed on the surface of the photocatalyst, upon exposing the photocatalysts to adequate light as shown in Fig. 10. which during the degradation process, the charge species such as OH^-, h^+, and e^- act as oxidizing and reducing agents, and $OH^{\cdot}$, $O_2^{\cdot}$, and $HO_2^{\cdot}$ radicals and holes (h^+) are intermediates that react spontaneously on the neighboring ions, and degrading the dye compounds to environmental friendly CO_2 and H_2O as shown at the following Equations.

$$\mathrm{TCA} + h\nu \rightarrow h^+ + e- \tag{3}$$

$$\mathrm{TCA} + O_2 \rightarrow O_2^{-} \tag{4}$$

$$O_2^{-} + 2H_2O \rightarrow 4OH^{\cdot} \tag{5}$$

$$h^+ + H_2O \rightarrow OH^{\cdot} + H^+ \tag{6}$$

$$H_2O + H^+ + O_2^{-} \rightarrow H_2O_2 + OH^{\cdot} \tag{7}$$

$$H_2O_2 + e^- \rightarrow OH^- + OH^{\cdot} \tag{8}$$

$$h^+ + OH^- \rightarrow OH^{\cdot} \tag{9}$$

$$OH^{\cdot} + \text{organic pollutant} \rightarrow \text{degradation to } CO_2 + H_2O \tag{10}$$

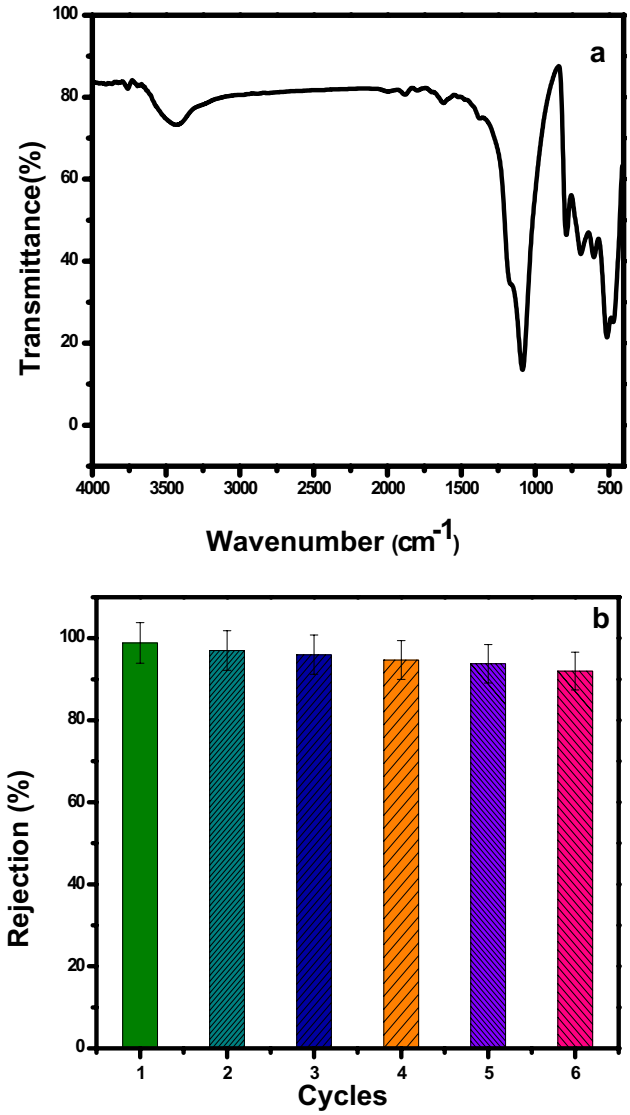

Figure 9. (**a**) FT-IR spectra and; (**b**) Reusability of TCA_2 after photocatalytic degradation for MB.

The developed photocatalyst, TiO_2/CuO@Ag has a p-n heterojunction formed as a result of the combination between p-type (CuO) and n-type (TiO_2) semiconductors. Furthermore, the conduction band (CB) level of TiO_2 is higher than the CB level of CuO. Leading to the diffusion of holes from p-type to n-type region and electrons from n-type to p-type via the heterojunctions or to the attached Ag nanoparticles. As a result, it makes the separation of photogenerated electrons and holes easier along with the influence of Ag nanoparticles' surface plasma resonance (SPR) that enhances the collection of visible light harvesting. Resulting in enhanced photocatalytic efficiency[39,49–51].

Conclusion

In conclusion, this study successfully synthesized a green-synthesized TiO_2/CuO@Ag nanocomposite using Nerium oleander leaves extract. The TCA nanocomposite exhibited superior photocatalytic activity for the degradation of MB under visible light. The presence of Ag in the nanocomposite significantly enhanced its photocatalytic efficiency, achieving a degradation percentage of 98.87% for MB. The TCA nanocomposite demonstrated stability and reusability, making it a promising material for environmental remediation applications. This research contributes to the development of sustainable and efficient photocatalytic materials for water treatment and pollution control. Further investigations can explore optimization and scalability of the TCA nanocomposite for broader environmental applications.

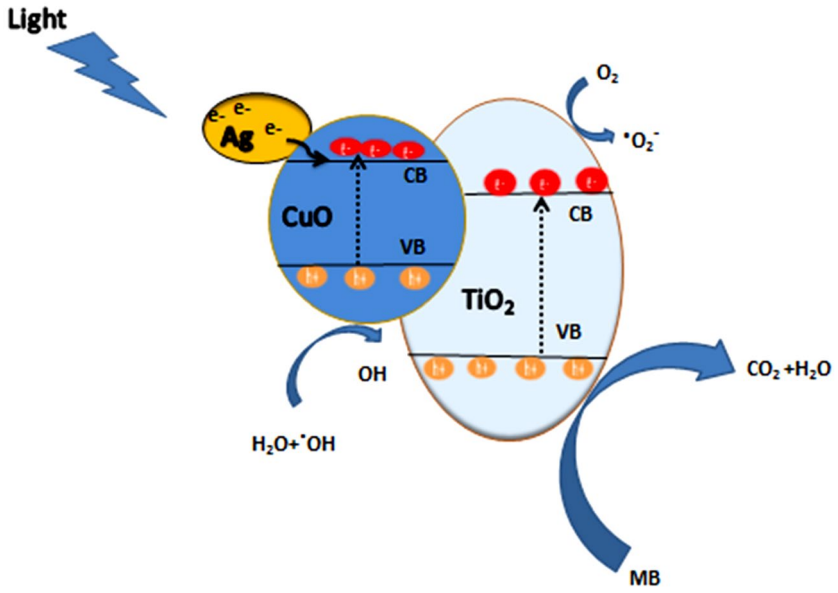

Figure 10. Schematic diagram of the mechanism for the photo catalytic of MB by TCANCs under visible light irradiation.

Data availability

All data underlying the results are available as part of the article and no additional source date are required.

Received: 29 September 2023; Accepted: 18 January 2024
Published online: 30 January 2024

References

1. Wang, M. *et al.* p–n Heterojunction photoelectrodes composed of Cu_2O-loaded TiO_2 nanotube arrays with enhanced photoelectrochemical and photoelectrocatalytic activities. *Energy Environ. Sci.* **6**, 1211–1220 (2013).
2. Zhang, Z. *et al.* IR-driven ultrafast transfer of plasmonic hot electrons in nonmetallic branched heterostructures for enhanced H_2 generation. *Adv. Mater.* **30**, 1705221 (2018).
3. Akpan, U. G. & Hameed, B. H. Parameters affecting the photocatalytic degradation of dyes using TiO_2-based photocatalysts: A review. *J. Hazard. Mater.* **170**, 520–529 (2009).
4. Elshypany, R. *et al.* Magnetic ZnO crystal nanoparticle growth on reduced graphene oxide for enhanced photocatalytic performance under visible light irradiation. *Molecules* **26**, 2269 (2021).
5. Mubarak, M. F., Selim, H. & Elshypany, R. Hybrid magnetic core–shell TiO_2@ $CoFe_3O_4$ composite towards visible light-driven photodegradation of Methylene blue dye and the heavy metal adsorption: Isotherm and kinetic study. *J. Environ. Health Sci. Eng.* **20**, 265–280 (2022).
6. Selim, H. *et al.* Superior photocatalytic activity of BaO@ Ag_3PO_4 nanocomposite for dual function degradation of methylene blue and hydrogen production under visible light irradiation. *Catalysts* **13**, 363 (2023).
7. Elaouni, A. *et al.* ZIF-8 metal organic framework materials as a superb platform for the removal and photocatalytic degradation of organic pollutants: A review. *RSC Adv.* **12**, 31801–31817 (2022).
8. Yu, C. *et al.* Novel fluorinated Bi_2MoO_6 nanocrystals for efficient photocatalytic removal of water organic pollutants under different light source illumination. *Appl. Catal. B Environ.* **209**, 1–11 (2017).
9. He, H. *et al.* Coupling electrochemical and biological methods for 17α-ethinylestradiol removal from water by different microorganisms. *J. Hazard. Mater.* **340**, 120–129 (2017).
10. Brillas, E. & Martínez-Huitle, C. A. Decontamination of wastewaters containing synthetic organic dyes by electrochemical methods. An updated review. *Appl. Catal. B Environ.* **166**, 603–643 (2015).
11. Ajmal, A. *et al.* Photocatalytic degradation of textile dyes on Cu_2O-CuO/TiO_2 anatase powders. *J. Environ. Chem. Eng.* **4**, 2138–2146 (2016).
12. Chen, J. E. *et al.* Synthesis of magnetic mesoporous titania colloidal crystals through evaporation induced self-assembly in emulsion as effective and recyclable photocatalysts. *Phys. Chem. Chem. Phys.* **17**, 27653–27657 (2015).
13. Zhang, Z., Huang, J., Zhang, M., Yuan, Q. & Dong, B. Ultrathin hexagonal SnS_2 nanosheets coupled with g-C_3N_4 nanosheets as 2D/2D heterojunction photocatalysts toward high photocatalytic activity. *Appl. Catal. B Environ.* **163**, 298–305 (2015).
14. Arfanis, M. K. *et al.* Photocatalytic properties of copper—modified core-shell titania nanocomposites. *J. Photochem. Photobiol. A Chem.* **370**, 145–155 (2019).
15. Liu, G., Wang, G., Hu, Z., Su, Y. & Zhao, L. Ag_2O nanoparticles decorated TiO_2 nanofibers as a pn heterojunction for enhanced photocatalytic decomposition of RhB under visible light irradiation. *Appl. Surf. Sci.* **465**, 902–910 (2019).
16. Wu, T. *et al.* Homogeneous doping of substitutional nitrogen/carbon in TiO_2 plates for visible light photocatalytic water oxidation. *Adv. Funct. Mater.* **29**, 1901943 (2019).
17. Sun, X., Yan, L., Xu, R., Xu, M. & Zhu, Y. Surface modification of TiO_2 with polydopamine and its effect on photocatalytic degradation mechanism. *Colloids Surf. A Physicochem. Eng. Asp.* **570**, 199–209 (2019).
18. Rekeb, L., Hamadou, L., Kadri, A., Benbrahim, N. & Chainet, E. Highly broadband plasmonic Cu film modified Cu_2O/TiO_2 nanotube arrays for efficient photocatalytic performance. *Int. J. Hydrog. Energy* **44**, 10541–10553 (2019).
19. Park, K.-R. *et al.* Design of highly porous SnO_2–CuO nanotubes for enhancing H_2S gas sensor performance. *Sens. Actuators B Chem.* **302**, 127179 (2020).

20. Wang, Y., Zhou, M., He, Y., Zhou, Z. & Sun, Z. In situ loading CuO quantum dots on TiO_2 nanosheets as cocatalyst for improved photocatalytic water splitting. *J. Alloys Compd.* **813**, 152184 (2020).
21. Shaislamov, U., Kim, H., Yang, J. M. & Yang, B. L. CuO/ZnO/TiO_2 photocathodes for a self-sustaining photocell: Efficient solar energy conversion without external bias and under visible light. *Int. J. Hydrog. Energy* **45**, 6148–6158 (2020).
22. Bathla, A., Rather, R. A., Poonia, T. & Pal, B. Morphology dependent photocatalytic activity of CuO/CuO–TiO_2 nanocatalyst for degradation of methyl orange under sunlight. *J. Nanosci. Nanotechnol.* **20**, 3123–3130 (2020).
23. Bae, J. Y. & Jang, S. G. Preparation and characterization of CuO—TiO_2 composite hollow nanospheres with enhanced photocatalytic activity under visible light irradiation. *J. Nanosci. Nanotechnol.* **19**, 6363–6368 (2019).
24. Singh, J., Mehta, A., Rawat, M. & Basu, S. Green synthesis of silver nanoparticles using sun dried tulsi leaves and its catalytic application for 4-Nitrophenol reduction. *J. Environ. Chem. Eng.* **6**, 1468–1474 (2018).
25. Thivaharan, V., Ramesh, V. & Raja, S. Green synthesis of silver nanoparticles for biomedical and environmental applications. In *Green Metal Nanoparticles: Synthesis, Characterization and their Applications*, 287–439 (2018).
26. Fatimah, I. & Herianto, R. Physicochemical characteristics and photocatalytic activity of silver nanoparticles-decorated on natural halloysite (An aluminosilicate clay). *Orient. J. Chem.* **34**, 857 (2018).
27. Durán, N. *et al.* Mechanistic aspects in the biogenic synthesis of extracellular metal nanoparticles by peptides, bacteria, fungi, and plants. *Appl. Microbiol. Biotechnol.* **90**, 1609–1624 (2011).
28. Zhu, J. *et al.* Highly dispersed CuO nanoparticles prepared by a novel quick-precipitation method. *Mater. Lett.* **58**, 3324–3327 (2004).
29. Etape, E. P., Ngolui, L. J., Foba-Tendo, J., Yufanyi, D. M. & Namondo, B. V. Synthesis and characterization of CuO, TiO_2, and CuO–TiO_2 mixed oxide by a modified oxalate route. *J. Appl. Chem* **2017**, 1–10 (2017).
30. Sebeia, N., Jabli, M. & Ghith, A. Biological synthesis of copper nanoparticles, using Nerium oleander leaves extract: Characterization and study of their interaction with organic dyes. *Inorgan. Chem. Commun.* **105**, 36–46 (2019).
31. Dharmadhas, J. S., Danaraj, J. & Packiavathy, I. A. S. V. Green fabrication of nerium oleander-mediated silver nanomaterials: Synthesis, structural, and stability analysis. *BioNanoScience* **13**, 1177–1183 (2023).
32. Bhadwal, A. S. *et al.* Biogenic synthesis and photocatalytic activity of CdS nanoparticles. *RSC Adv.* **4**, 9484–9490 (2014).
33. Khoshnevisan, B., Marami, M. B. & Farahmandjou, M. Fe3+-doped anatase TiO_2 study prepared by new sol-gel precursors. *Chin. Phys. Lett.* **35**, 027501 (2018).
34. El-Trass, A., ElShamy, H., El-Mehasseb, I. & El-Kemary, M. CuO nanoparticles: Synthesis, characterization, optical properties and interaction with amino acids. *Appl. Surf. Sci.* **258**, 2997–3001 (2012).
35. Sundar, S., Venkatachalam, G. & Kwon, S. J. Biosynthesis of copper oxide (CuO) nanowires and their use for the electrochemical sensing of dopamine. *Nanomaterials* **8**, 823 (2018).
36. Wang, G., Xu, L., Zhang, J., Yin, T. & Han, D. Enhanced photocatalytic activity of powders (P25) via calcination treatment. *Int. J. Photoenergy*,**50**, 1–9 (2012).
37. Devaraj, P., Kumari, P., Aarti, C. & Renganathan, A. Synthesis and characterization of silver nanoparticles using cannonball leaves and their cytotoxic activity against MCF-7 cell line. *J. Nanotechnol.*,**6**, 1–5 (2013).
38. El Sharkawy, H. M., Shawky, A. M., Elshypany, R. & Selim, H. Efficient photocatalytic degradation of organic pollutants over TiO_2 nanoparticles modified with nitrogen and MoS_2 under visible light irradiation. *Sci. Rep.* **13**, 8845 (2023).
39. Lu, D. *et al.* Synthesis and photocatalytic activities of a CuO/TiO_2 composite catalyst using aquatic plants with accumulated copper as a template. *RSC Adv.* **9**, 2018–2025 (2019).
40. Velliyan, S. & Murugesan, K. S. Synthesis and study on structural, morphological, optical properties and photocatalytic activity of CuO: Erx3+ photocatalysts. *Chin. J. Phys.* **77**, 2425–2434 (2022).
41. Hou, Y., Li, X., Zhao, Q., Quan, X. & Chen, G. TiO_2 nanotube/Ag–AgBr three-component nanojunction for efficient photoconversion. *J. Mater. Chem.* **21**, 18067–18076 (2011).
42. Basumatary, R., Konwar, D., Basumatary, B. & Ramchiary, A. Plasmonic enhanced branched Ag sensitized Cu_2O–CuO/TiO_2 heterojunction with unprecedented photocatalytic degradation under visible light. *J. Phys. Chem. Solids* **180**, 111435 (2023).
43. Liu, Y. *et al.* Enhanced visible light photo-Fenton-like degradation of tetracyclines by expanded perlite supported $FeMo_3Ox$/g-C3N4 floating Z-scheme catalyst. *J. Hazard. Mater.* **424**, 127387 (2022).
44. Koohestani, H. & Sadrnezhaad, S. K. Photocatalytic degradation of methyl orange and cyanide by using TiO_2/CuO composite. *Desalin. Water Treat.* **57**, 22029–22038 (2016).
45. Zhang, X. *et al.* A bamboo-inspired hierarchical nanoarchitecture of Ag/CuO/TiO_2 nanotube array for highly photocatalytic degradation of 2, 4-dinitrophenol. *J. Hazard. Mater.* **313**, 244–252 (2016).
46. Rajendran, R. *et al.* g-C_3N_4/TiO_2/CuO S-scheme heterostructure photocatalysts for enhancing organic pollutant degradation. *J. Phys. Chem. Solids* **161**, 110391 (2022).
47. Sobahi, T. R., Abdelaal, M. Y., Mohamed, R. & Mokhtar, M. Photocatalytic degradation of methylene blue dye in water using Pt/ZnO-MWCNT under visible light. *Nanosci. Nanotechnol. Lett.* **9**, 144–150 (2017).
48. Adarsha, J. *et al.* Hydrothermal synthesis of novel heterostructured Ag/TiO_2/$CuFe_2O_4$ nanocomposite: Characterization, enhanced photocatalytic degradation of methylene blue dye, and efficient antibacterial studies. *Water Environ. Res.* **94**, e10744 (2022).
49. Lin, D., Wu, H., Zhang, R. & Pan, W. Enhanced photocatalysis of electrospun Ag–ZnO heterostructured nanofibers. *Chem. Mater.* **21**, 3479–3484 (2009).
50. Zelekew, O. A. & Kuo, D.-H. A two-oxide nanodiode system made of double-layered p-type Ag_2O@ n-type TiO_2 for rapid reduction of 4-nitrophenol. *Phys. Chemi. Chem. Phys.* **18**, 4405–4414 (2016).
51. Fouda, A., Salem, S. S., Wassel, A. R., Hamza, M. F. & Shaheen, T. I. Optimization of green biosynthesized visible light active CuO/ZnO nano-photocatalysts for the degradation of organic methylene blue dye. *Heliyon* **6**, 1–13 (2020).

Author contributions

H.M., A.M., R.E., M.F.M. and H.S., assisted in the experimental work, including the characterization of the nanocomposite. Participated in data analysis and interpretation. Contributed to the literature review and discussion of the results. Reviewed and revised the manuscript. M.F.M., H.M. and H.S., Conceived and designed the research study, supervised the experimental work and data analysis,.Contributed to the interpretation of the results and Co-wrote and revised the manuscript H.S. made writing-review and editing. All authors have read and approved the final version of the manuscript.

Funding

Open access funding provided by The Science, Technology & Innovation Funding Authority (STDF) in cooperation with The Egyptian Knowledge Bank (EKB). This research received no external funding.

Competing interests

The authors declare no competing interests.

Additional information

Correspondence and requests for materials should be addressed to H.M.E.S. or H.S.

Reprints and permissions information is available at www.nature.com/reprints.

Publisher's note Springer Nature remains neutral with regard to jurisdictional claims in published maps and institutional affiliations.